Structure Elucidation

International Edition: DOI: 10.1002/anie.201500518
German Edition: DOI: 10.1002/ange.201500518

Superstructure of a Substituted Zeolitic Imidazolate Metal–Organic Framework Determined by Combining Proton Solid-State NMR Spectroscopy and DFT Calculations**

Maria Baias, Anne Lesage, Sonia Aguado, Jerome Canivet, Virginie Moizan-Basle, Nathalie Audebrand, David Farrusseng, and Lyndon Emsley**

Abstract: *We report the supercell crystal structure of a ZIF-8 analog substituted imidazolate metal–organic framework (SIM-1) obtained by combining solid-state nuclear magnetic resonance and powder X-ray diffraction experiments with density functional theory calculations.*

The introduction of metal–organic frameworks (MOFs) has provided crystalline porous materials with an extremely wide range of three-dimensional topologies leading to outstanding properties.[1] An important category of MOFs are the zeolite imidazolate frameworks (ZIFs) in which the metal-oxide units are linked by imidazolate moities and which display structural features similar to zeolitic materials.[2] In particular ZIFs can be remarkable frameworks for CO_2 adsorption and gas separation.[3] The most promising candidates contain imidazolates functionalized with polar moities like ZIF-78 and 82, or with asymmetric imidazolates functionalized at position 4 and 5, such as ZIF-93, 96, and 97.[4] It has been shown that the symmetry of the organic linker as well as the polarizability of the functional group have a significant influence over the uptake capacity and separation selectivity of a given ZIF topology.[4,5]

Beyond the nature of the organic fragments, the properties of MOFs, as is the case for most functional materials, are related to their atomic-scale structure. The size of the pores is for example a critical structural parameter for gas capture.[6] Single-crystal X-ray diffraction techniques are in principle the method of choice to elucidate the structure of these crystalline materials. However this becomes much more difficult when crystals for diffraction are unobtainable, when the structure contains some disorder or partial functionalization, or when unit cells are large.

Solid-state NMR spectroscopy complements diffraction methods and has developed into a powerful tool to solve crystal structures of inorganic or molecular solids.[7] As such, this spectroscopy has been extensively used to investigate structural features in MOFs, to characterize conformation changes upon adsorption of probe molecules or to study the dynamic events that govern host–guest interactions in these frameworks.[8]

Particular advances have recently been made in the interpretation of solid-state NMR spectra by combining sophisticated spectral assignment strategies with state-of-the-art density functional theory (DFT) chemical shift calculation methods. While for powdered organic samples protocols were first demonstrated using ^{13}C and ^{15}N spectra,[9] it has also been shown that first-principles calculations could very well reproduce measured proton chemical shifts, and that the latter provide very sensitive structural probes.[7e,10] Proton solid-state NMR spectroscopy in combination with crystal-structure prediction and shift calculation was recently used to determine the structure of an organic compound of previously unknown structure.[7f]

Here we use high-resolution ^1H solid-state NMR spectroscopy in combination with first-principles shift calculations to resolve the crystal structure of a new substituted imidazolate material (SIM-1),[11] in which the small pore sizes together with the presence of polar groups makes the material an ideal candidate for CO_2 separation, and for which single crystals could not be obtained. Based on the powder X-ray diffraction patterns (PXRD), it can be seen that the crystal structure of SIM-1 is analog to those of ZIF-8[2] and ZIF-90[12] with a sodalite topology composed of four- and six-membered rings in which the metal ions (M) of the cage, here Zn atoms, are linked by 4-methyl-5-imidazolecarboxaldehyde moieties (Figure 1).

Characterization of the material by thermal gravimetric analysis (TGA), scanning electron microscopy (SEM), solution NMR spectroscopy and elemental analysis, as well as gas adsorption measurements indicate a high purity of the powder (see the Supporting Information). In the following we show

[*] Dr. M. Baias, Dr. A. Lesage, Prof. L. Emsley
Institut des Sciences Analytiques
Centre de RMN à très hauts champs (CNRS/ENS-Lyon, UCB-Lyon1)
Université de Lyon, 69100 Villeurbanne (France)
E-mail: lyndon.emsley@ens-lyon.fr
Dr. S. Aguado, Dr. J. Canivet, Dr. D. Farrusseng
IRCELYON, Institut de Recherches sur la Catalyse et l'Environnement de Lyon, 69626 Villeurbanne (France)
E-mail: david.farrusseng@ircelyon.univ-lyon1.fr
Dr. V. Moizan-Basle
IFP Energies nouvelles, 69360 Solaize Cedex (France)
Dr. N. Audebrand
Université Européenne de Bretagne, Université de Rennes 1
Institut des Sciences Chimiques de Rennes, UMR CNRS 6226
35042 Rennes Cedex (France)
Prof. L. Emsley
Institut des Sciences et Ingénierie Chimiques
Ecole Polytechnique Fédérale de Lausanne (EPFL)
1015 Lausanne (Switzerland)

[**] Financial support from the IR RMN THC FRE 3050 for conducting the research is gratefully acknowledged.

Supporting information for this article is available on the WWW under http://dx.doi.org/10.1002/anie.201500518.

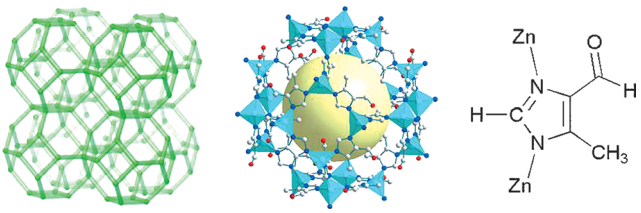

Figure 1. The sodalite topology (left) and of the framework of SIM-1 (middle), and of the substituted imidazolate linker (right). The yellow ball corresponds to the pore size.

how the comparison between observed and calculated proton chemical shifts and measured ^{1}H-^{1}H proximities allows us to exclude several simple structures generated from the possible relative orientations of the imidazolate ring and of the aldehyde group, and leads to the proposition of a superstructure that is in agreement with all the experimental data. Although the PXRD pattern was unable to discriminate between the various possible structures, the proposed superstructure is in agreement with the experimentally recorded PXRD pattern, further validating the approach developed here.

Figure 2a shows the one-dimensional (1D) ^{1}H solid-state NMR spectrum of SIM-1 recorded at high magnetic field (800 MHz) and with very fast magic angle spinning (60 kHz MAS, magic angle spinning).

The resonance at around 3.9 ppm can be readily assigned to water molecules trapped in the framework based on the comparison between ^{1}H spectra of SIM-1 samples with different amounts of hydration (see Figure S8 in the Supporting Information). The remaining six chemical shifts correspond to the three different types of protons in the substituted imidazolate linker, namely the aldehyde (9.62 and 9.31 ppm), the imidazolate (7.10 and 7.80 ppm), and the methyl protons (2.23 and 1.83 ppm). Two distinct resonances are observed for each type of protons in a 1:1 intensity ratio, indicating the presence of two, equally probable, different local geometries within the framework. The connectivities between the three types of protons within a given imidazolate linker were established using ^{1}H-^{13}C INEPT[14] and long-range HETCOR spectra with eDUMBO-1_{22} homonuclear decoupling,[15] both spectra recorded under 22 kHz MAS (shown in Figure S9). The procedure is detailed in the Supporting Information. The determined connectivities are depicted schematically in Figure 2a in blue and orange. Figure 2b shows the two-dimensional double-quantum (DQ)–single-quantum (SQ) proton correlation spectrum of SIM-1 recorded with 60 kHz MAS. Several correlations are observed between protons belonging to the two different types of imidazolate units (indicated in red). Notably, strong correlations are visible between the two types of imidazolate (Im) protons at $(\omega_1, \omega_2) = (14.9\text{ ppm}, 7.10\text{ ppm})$ and at $(\omega_1, \omega_2) = (14.9\text{ ppm}, 7.80\text{ ppm})$, while auto-correlation peaks along the $\omega_1 = 2\omega_2$ diagonal are of much weaker intensity for those protons. These correlations indicate a spatial proximity between the Im protons of the two structurally distinct linkers. This observation provides a strong geometrical constraint on the structure. This, together with the chemical shifts, is used to discriminate between various possible structures as described

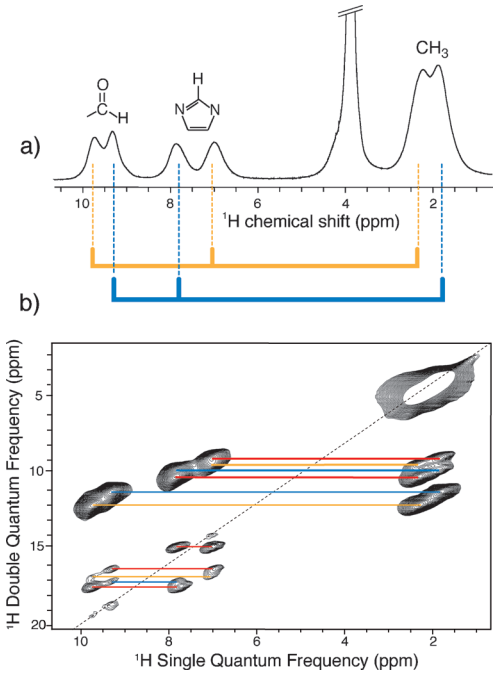

Figure 2. a) ^{1}H NMR spectrum of SIM-1. Connectivities between protons of a given imidazolate linker are indicated schematically in blue and orange. b) 2D DQ-SQ ^{1}H spectrum of SIM-1, recorded with a rotor-synchronized BABA[13] scheme for excitation and reconversion blocks. Correlations between the protons of the two different kinds of linkers are indicated in red, while connectivties between protons belonging to the same type of units (including intra-linker correlations) are shown in blue and orange. The different correlations were assigned as described in the text. Both spectra were recorded at a MAS frequency of 60 kHz. The same correlations are observed in the presence or absence of water molecules within the framework (Figure S8).

in the following. Weak distributions of isotropic chemical shifts are observed in both ^{13}C and ^{1}H spectra, indicating only small variations of local environments at each site and thus a well-ordered material. We also note that there is no indication of any dynamical processes from the ^{1}H and ^{13}C NMR spectra, which remain unchanged over a temperature range of −50 to 65 °C.

In order to elucidate the atomic-scale geometry of SIM-1, the ensemble of the six possible basic structures were envisaged, for each of which we performed DFT calculations of the proton chemical shifts using the CASTEP code[16] within the GIPAW formalism.[17] To generate the candidate structures we started from the known crystal structure of ZIF-8 (space group $I\bar{4}3m$; $a = 16.99$ Å) and reduced the symmetry to I23 such that we could replace the functional group with that of SIM-1. The different structures were generated by varying the relative orientations of the five-membered rings and/or of the aldehyde groups in the six-membered hexagonal Zn rings, followed by DFT geometry optimization. The resulting six candidate structures (**I**–**VI**) are depicted schematically in Figure 3. The corresponding crystal structures are shown in Figures S10–S15.

- Structure **I**: The aromatic rings and the aldehyde groups have the same orientation, the proton of the aldehyde points towards the methyl group of the same Im fragment.

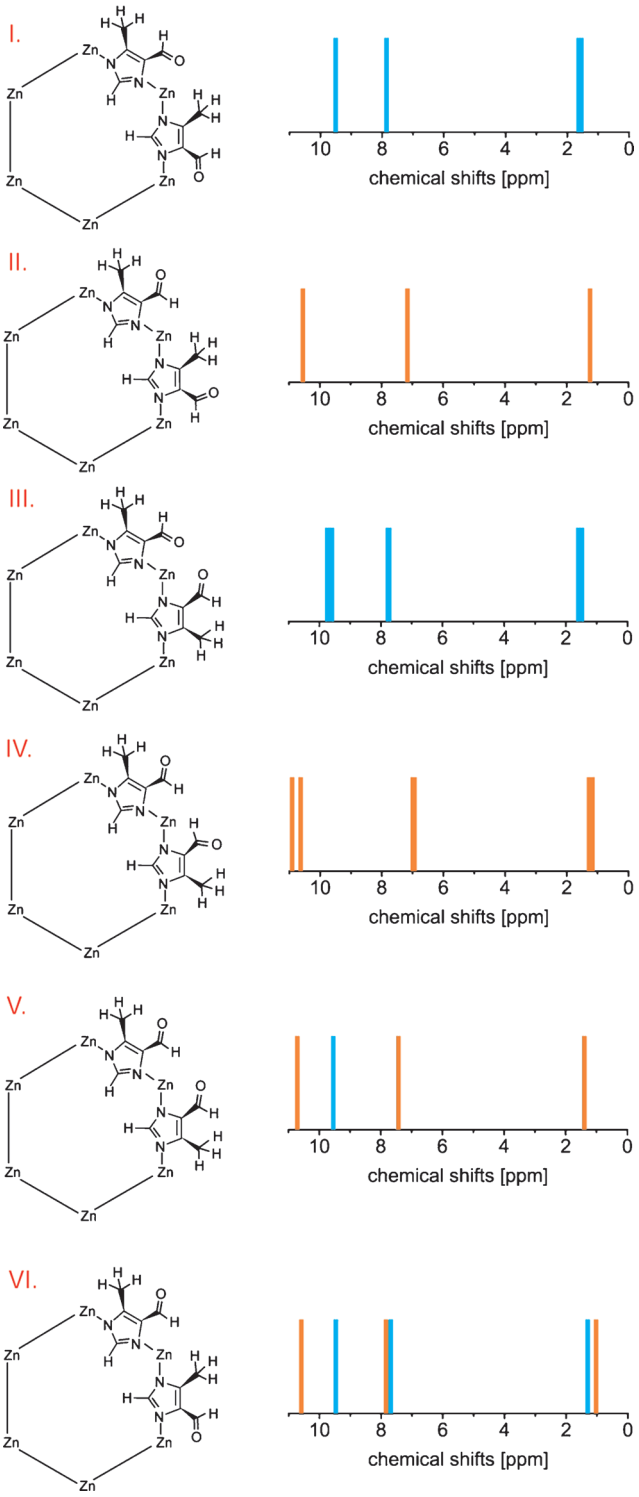

Figure 3. The six calculated structures together with the corresponding calculated proton NMR spectra. The space group is I23 for **I** and **II**, and P23 for **III** to **VI**.

- Structure **II**: The aromatic rings and the aldehyde groups have the same orientation, the proton of the aldehyde pointing away from the methyl group of the same Im fragment.
- Structure **III**: The aromatic rings have alternating orientations where the OH of the aldehyde group of one ring in the hexagon is close to the OH of the aldehyde of the neighboring ring. All aldehyde groups have the same orientation, the proton of the aldehyde pointing towards the methyl group of the same Im fragment.
- Structure **IV**: The aromatic rings have alternating orientations where the OH of the aldehyde group of one ring in the hexagon is close to the OH of the aldehyde of the neighboring ring. All aldehyde groups have the same orientation, the proton of the aldehyde pointing away from the methyl group of the same Im fragment.
- Structure **V**: The aromatic rings have alternating orientations where the OH of the aldehyde group of one ring in the hexagon is close to the OH of the aldehyde of the neighboring ring. The orientation of the aldehyde group also changes from one unit to the next.
- Structure **VI**: All aromatic rings have the same orientation, as in **I** and **II**, but the orientation of the aldehyde group is changing from one unit to the next in the hexagon.

To determine whether one of these structures correspond to that of SIM-1, the calculated ^{1}H chemical shift values were compared to the experimentally measured shifts. The ^{1}H NMR spectra predicted from DFT chemical shift calculations are shown in Figure 3 for each of the six structures. Structures **I** and **II** yield only a single set of chemical shifts. This is expected since inspection of the structures reveals that the three types of protons are in the same environment from one linker to another. The calculated NMR spectra of **III** and **IV** do not match the experimental spectrum, as only very small chemical shift differences if any, are predicted for the different imidazolate, aldehyde, and methyl protons. This is in agreement with the observation that, despite the fact that the orientation of the rings alternates from one linker to the other, the local environment of the three types of protons is not very different, with functional groups where the H or the O atom of the aldehyde groups always points towards the CH_3 moiety (structures **III** and **IV**, respectively). Two distinct chemical shifts are calculated for the aldehyde proton of **V**. This is again expected as these protons are now subjected to two quite different local environments, one pointing towards the OH group of the neighboring fragment, the second towards the CH_3 group of the same unit. A single set of chemical shifts is however observed for the Im and CH_3 protons, indicating that structure **V** is not correct. The calculated proton NMR spectrum of **VI** yields two distinct chemical shifts for the imidazolate, the aldehyde and the methyl protons, and from this point of view matches relatively well the experimental spectrum.

To further test **VI** as a potential structure, the intra- and interlinker ^{1}H-^{1}H distances (Table S2) were calculated and compared to the correlations observed in the 2D DQ-SQ spectrum of Figure 2b. The calculated internuclear distances between the imidazolate protons are however not in agreement with the proximities observed in the 2D spectrum. In particular, the shortest distances between two imidazolate protons observed in structure **VI** correspond to nuclei belonging to the same type of organic linker (Table S2 and Figure S15), and cannot account for the strong correlations observed between the two different kinds of Im protons. This

discrepancy clearly indicates that **VI** is not a structure of SIM-1. Thus, none of the basic structures is in agreement with the experimental ^{1}H NMR data. We note that a structure where all the orientations of the rings and of the aldehyde groups would be randomly present is excluded as this would lead to a broad distribution of proton chemical shifts between 7 and 11 ppm in the ^{1}H NMR spectrum. Any attempt to generate two different local geometries for linkers having the same basic configuration were not conclusive, as was the case for structures incorporating water molecules. We thus presume that the structure must be a superstructure made up of two units.

As the sum of the ^{1}H NMR spectra of **I** and **II** matches the experimental spectrum well, we propose a further candidate structure by combining **I** and **II** (with equal population) into a $2\times2\times2$ supercell structure ($a = 33.487$ Å), structure **VII**. Starting from the crystal structure of **I** and based on the symmetry operations allowed by the I23 space group, the orientation of half of the aldehyde groups was changed by 180°, in such a way that the four-membered Zn rings be composed of successive linkers of different geometry. This latter ensures that the structure will have the proximities as observed in the DQ-SQ correlation experiments. The supercell structure is shown in Figure 4. It is the only $2\times2\times2$ supercell structure that combines **I** and **II** and which also satisfies the structural constraints observed experimentally. The protons colored in cyan and white belong to imidazolate units having the same local geometry as the linkers of structures **I** and **II**, respectively. While in structure **VI** the linkers with the two different local geometries alternate within the hexagonal rings, we observe that the following arrangements are present in the six-membered Zn rings of **VII**: hexagons containing six linkers with the aldehyde orientation of **I**; hexagons containing three linkers with the aldehyde orientation of **I** and three linkers with the aldehyde orientation of **II**, with the two possible orders for the linkers in the hexagon: **I-II-I-II-I-II** and **I-I-II-I-II-II**; and hexagons containing two linkers with the aldehyde orientation of **I** and four linkers with the aldehyde orientation of **II** and the following order of the linkers in the hexagon **I-II-II-II-II-I**.

This new structure matches the NMR data well. Figure 5a illustrates the good agreement between the proton spectrum of SIM-1 and the predicted spectrum of **VII**, as computed from the sum of the NMR spectra of **I** and **II**. (The differences observed between experiment and calculation are within what we would expect for methyl groups and H-bonded protons at the accuracy achieved by DFT today.) In addition, the shortest distance between the imidazolate protons is now obtained for the two structurally distinct organic linkers (Table S3), which is fully consistent with the corresponding correlations observed in the DQ-SQ spectrum. The other experimentally observed ^{1}H-^{1}H connectivities are also in line with the calculated distances. The superstructure reveals that the substituents point towards the center of the cavity, leading to a pore size of about 7.5 Å.

Finally the space group of **VII** (I23) corresponds to one of the possible space groups for SIM-1 (*I*23, *I*432, $I\bar{4}3m$, $Im\bar{3}$, $Im\bar{3}m$) from PXRD indexing and intensity extraction (Le Bail fit), and that the calculated PXRD pattern of **VII** reproduces

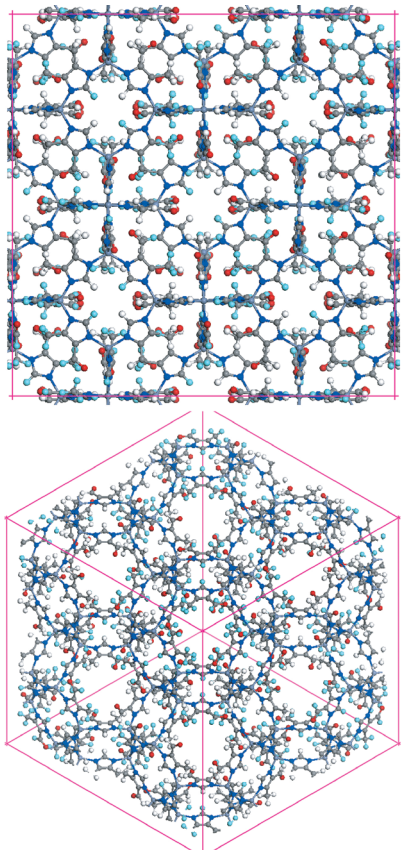

Figure 4. Crystal structure of the supercell structure **VII**. (N, blue; O, red; C, gray; H, white and cyan). Two different views are shown to highlight the square and hexagonal arrangements of the sodalite cage. Protons corresponding to the two structurally different linkers are shown in white and cyan, respectively.

the experiment well, as shown in Figure 5b. The match is significantly improved with respect to comparisons with the simulated patterns of the six initially generated basic structures (Figures S10–S15).

The pattern matching of the experimental PXRD pattern and their indexing for either a small cell ($a = 15.7276$ Å) or the supercell proposed here ($a = 33.4528$ Å) with space group I23 are shown in Figure S16. In both cases all of the observed reflections are predicted. For the supercell, several additional reflections are possible, but are not observed experimentally. This is confirmed by the predicted PXRD pattern from structure **VII**, where we see a good agreement with the experiment (Figure 5b). Notably, we can rationalize the very low (essentially zero) predicted intensities for many lines since the different orientations of the aldehyde and formyl groups concern only few atoms (two oxygen and two hydrogen atoms). Indeed, only 3% of the electrons change positions between structure **I** (or **II**) in a small cell and the supercell structure **VII**. This highlights the complementarity of the global nature of PXRD with the local site-specific information from NMR spectroscopy. We have observed some changes in peak intensities as a function of the synthesis and/or washing conditions of the material. Details are provided in Table S1 and Figure S7. These variations in

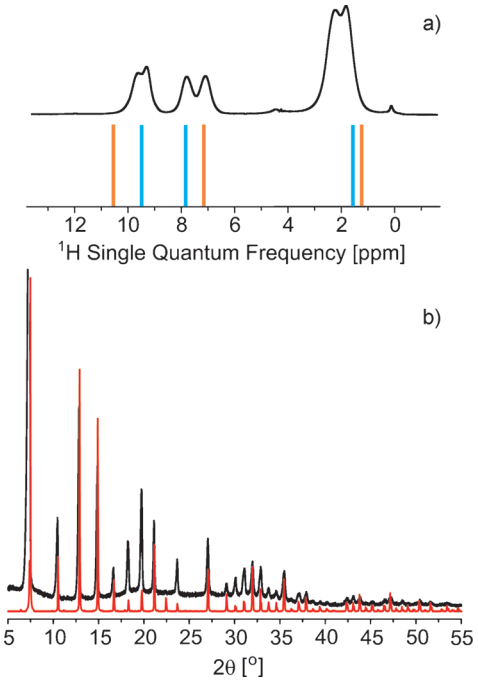

Figure 5. a) Comparison between experimental ^{1}H NMR spectrum of SIM-1 (upper) and the predicted spectrum of the supercell **VII** (lower) as obtained from the addition of the DFT-calculated chemicals shifts of **I** (blue) and **II** (orange). b) Comparison between the experimentally recorded powder X-ray diffraction pattern (black) of SIM-1 and that calculated for the supercell (red).

peak intensity likely come from differences in the occupancy of the pores between MOFs subjected to different synthesis conditions, with possibly molecules within the pores.

Furthermore, computed energies from DFT (shown in Figure S17) clearly show that structures **I** and **II** are predicted to be the most stable conformers for the aldehyde groups, further validating the superstructure determined here.

In conclusion, a supercell structure for the substituted imidazolate material, SIM-1, was determined from the combination of NMR experiments and chemical shift calculations. Unexpected structural features were found, with organic linkers of two distinct local geometries, and a specific arrangement of these linkers within the framework. The structure reveals a cavity of 7.5 Å in diameter, which is inconsistent with N_2 adsorption experimental results.[11] This small pore size together with the presence of polar groups makes this material an ideal candidate for CO_2 separation, which will be reported elsewhere.

Experimental Section

All solid-state NMR experiments were recorded on a Bruker Avance III spectrometer operating at ^{1}H and ^{13}C Larmor frequencies of 800 MHz and 201 MHz, respectively. 1D ^{1}H spectra were recorded with a 1.3 mm triple resonance probe with 60 kHz MAS. 1D ^{13}C cross-polarization (CP) MAS spectra were recorded with a 3.2 mm triple resonance probe at 22 kHz MAS. ^{1}H chemical shifts were referenced to the single resonance observed for protons in adamantane at 1.87 ppm with respect to the signal for neat tetramethylsilane (TMS). ^{13}C chemical shifts were referenced to the CH_2 resonance observed for adamantane at 38.48 ppm with respect to the signal for neat TMS. The ^{1}H DQ MAS experiment was recorded with a 1.3 mm triple resonance probe at 60 kHz MAS with a ^{1}H 90° pulse duration of 2 μs. One rotor period of the back-to-back (BABA) recoupling sequence ($90°x-\tau-90°-x-90°y-\tau-90°-y$, where $\tau=\tau_R/2$ minus the pulse durations) was used for excitation and reconversion of DQ coherence. 768 increments of 32 transients each were acquired, with an acquisition time in t_2 of 20 ms, and a repetition delay of 2 s was used, resulting in a total experimental time of 14 h. The spectrum was recorded in a rotor-synchronized fashion in t_1. The states-TPPI procedure was used for quadrature detection in the indirect dimension for all two-dimensional experiments. First-principles calculations were performed using the academic version number 5.5 of the CASTEP software package, which uses plane-wave basis sets and ultrasoft pseudopotentials. All calculations used PBE exchange-correlation functional within the generalized gradient approximation. Geometry optimizations were performed starting from the X-ray diffraction crystal structure of ZIF-8 (CSD entry code: OFERUN), and replacing the functional groups with those specific to the SIM-1 structure. The unit cell was constrained to the cell dimensions determined from powder X-ray diffraction experiments on SIM-1. The initial framework was optimized for all atoms positions, while the subsequent structures were only optimized for the functional groups, the positions and orientations of which vary to generate several possible structures. The NMR chemical shifts were computed using the gauge-including projector augmented wave (GIPAW) method implemented in CASTEP. All calculations were performed at the gamma point in the Brillouin zone using a maximum planewave cut-off energy of 550 eV. The chemical shieldings σ_{calc} were converted into calculated chemical shifts δ_{calc} using the relation $\delta_{calc}=\sigma_{ref}-\sigma_{calc}$ with the value of σ_{ref} determined by a linear regression between calculated and experimental shifts, imposing a slope of unity. A CASTEP calculation of the chemical shifts of structure VII was not possible because the unit cell consists of 2640 atoms and calculating such a large structure requires more computing memory than available so far.

Keywords: density functional calculations · metal–organic frameworks · porous materials · solid-state NMR spectroscopy · X-ray diffraction

How to cite: *Angew. Chem. Int. Ed.* **2015**, *54*, 5971–5976
Angew. Chem. **2015**, *127*, 6069–6074

[1] M. Eddaoudi, J. Kim, N. Rosi, D. Vodak, J. Wachter, M. O'Keefe, O. Yaghi, *Science* **2002**, *295*, 469.
[2] K. S. Park, Z. Ni, A. P. Côté, J. Y. Choi, R. Huang, F. J. Uribe-Romo, H. K. Chae, M. O'Keeffe, O. M. Yaghi, *Proc. Natl. Acad. Sci. USA* **2006**, *103*, 10186–10191.
[3] a) R. Banerjee, A. Phan, B. Wang, C. Knobler, H. Furukawa, M. O'Keeffe, O. M. Yaghi, *Science* **2008**, *319*, 939–943; b) R. Banerjee, H. Furukawa, D. Britt, C. Knobler, M. O'Keeffe, O. M. Yaghi, *J. Am. Chem. Soc.* **2009**, *131*, 3875–3877; c) N. T. T. Nguyen, H. Furukawa, F. Gándara, H. T. Nguyen, K. E. Cordova, O. M. Yaghi, *Angew. Chem. Int. Ed.* **2014**, *53*, 10645–10648; *Angew. Chem.* **2014**, *126*, 10821–10824.
[4] W. Morris, B. Leung, H. Furukawa, O. K. Yaghi, N. He, H. Hayashi, Y. Houndonougbo, M. Asta, B. B. Laird, O. M. Yaghi, *J. Am. Chem. Soc.* **2010**, *132*, 11006–11008.
[5] H. Amrouche, S. Aguado, J. Pérez-Pellitero, C. L. Chizallet, F. Siperstein, D. Farrusseng, N. Bats, C. Nieto-Draghi, *J. Phys. Chem. C* **2011**, *115*, 16425–16432.
[6] L. J. Murray, M. Dinca, J. R. Long, *Chem. Soc. Rev.* **2009**, *38*, 1294–1314.
[7] a) D. H. Brouwer, R. J. Darton, R. E. Morris, M. H. Levitt, *J. Am. Chem. Soc.* **2005**, *127*, 10365–10370; b) T. Loiseau, L.

Lecroq, C. Volkringer, J. Marrot, G. Férey, M. Haouas, F. Taulelle, S. Bourrelly, P. L. Llewellyn, M. Latroche, *J. Am. Chem. Soc.* **2006**, *128*, 10223 – 10230; c) B. Elena, G. Pintacuda, N. Mifsud, L. Emsley, *J. Am. Chem. Soc.* **2006**, *128*, 9555 – 9560; d) E. Salager, R. S. Stein, C. J. Pickard, B. Elena, L. Emsley, *Phys. Chem. Chem. Phys.* **2009**, *11*, 2610 – 2621; e) M. Baias, C. M. Widdifield, J.-N. Dumez, H. P. G. Thompson, T. G. Cooper, E. Salager, S. Bassil, R. S. Stein, A. Lesage, G. M. Day, L. Emsley, *Phys. Chem. Chem. Phys.* **2013**, *15*, 8069 – 8080; f) M. Baias, J.-N. Dumez, P. H. Svensson, S. Schantz, G. M. Day, L. Emsley, *J. Am. Chem. Soc.* **2013**, *135*, 17501 – 17507; g) L. Mafra, S. M. Santos, R. Siegel, I. Alves, F. A. Almeida Paz, D. Dudenko, H. W. Spiess, *J. Am. Chem. Soc.* **2012**, *134*, 71 – 74; h) K. Kalakewich, R. Iuliucci, J. K. Harper, *Cryst. Growth Des.* **2013**, *13*, 5391 – 5396.

[8] a) Y. Jiang, J. Huang, B. Kasumaj, G. Jeschke, M. Hunger, T. Mallat, A. Baiker, *J. Am. Chem. Soc.* **2009**, *131*, 2058 – 2059; b) X. Kong, E. Scott, W. Ding, J. A. Mason, J. R. Long, J. A. Reimer, *J. Am. Chem. Soc.* **2012**, *134*, 14341 – 14344; c) S. Devautour-Vinot, G. Maurin, C. Serre, P. Horcajada, D. P. da Cunha, V. Guillerm, E. d. S. Costa, F. Taulelle, C. Martineau, *Chem. Mater.* **2012**, *24*, 2168 – 2177; d) X. Kong, H. Deng, F. Yan, J. Kim, J. A. Swisher, B. Smit, O. M. Yaghi, J. A. Reimer, *Science* **2013**, *341*, 882 – 885; e) C. R. Murdock, N. W. McNutt, D. J. Keffer, D. M. Jenkins, *J. Am. Chem. Soc.* **2014**, *136*, 671 – 678.

[9] a) C. Bonhomme, C. Gervais, F. Babonneau, C. Coelho, F. Pourpoint, T. Azaïs, S. E. Ashbrook, J. M. Griffin, J. R. Yates, F. Mauri, C. J. Pickard, *Chem. Rev.* **2012**, *112*, 5733 – 5779; b) J. C. Facelli, D. M. Grant, *Nature* **1993**, *365*, 325 – 327; c) A. C. de Dios, J. G. Pearson, E. Oldfield, *Science* **1993**, *260*, 1491 – 1496.

[10] a) A. Rapp, I. Schnell, D. Sebastiani, S. P. Brown, V. Percec, H. W. Spiess, *J. Am. Chem. Soc.* **2003**, *125*, 13284 – 13297; b) J. Yates, S. Dobbins, C. Pickard, F. Mauri, P. Ghi, R. Harris, *Phys. Chem. Chem. Phys.* **2005**, *7*, 1402 – 1407; c) J. R. Yates, T. N. Pham, C. J. Pickard, F. Mauri, A. M. Amado, A. M. Gil, S. P. Brown, *J. Am. Chem. Soc.* **2005**, *127*, 10216 – 10220; d) N. Mifsud, B. Elena, C. J. Pickard, A. Lesage, L. Emsley, *Phys. Chem. Chem. Phys.* **2006**, *8*, 3418; e) E. Salager, G. M. Day, R. S. Stein, C. J. Pickard, B. Elena, L. Emsley, *J. Am. Chem. Soc.* **2010**, *132*, 2564 – 2566.

[11] S. Aguado, J. Canivet, D. Farrusseng, *Chem. Commun.* **2010**, *46*, 7999 – 8001.

[12] W. Morris, C. J. Doonan, H. Furukawa, R. Banerjee, O. M. Yaghi, *J. Am. Chem. Soc.* **2008**, *130*, 12626 – 12627.

[13] I. Schnell, A. Lupulescu, S. Hafner, D. E. Demco, H. W. Spiess, *J. Magn. Reson.* **1998**, *133*, 61 – 69.

[14] B. Elena, A. Lesage, S. Steuernagel, A. Bockmann, L. Emsley, *J. Am. Chem. Soc.* **2005**, *127*, 17296 – 17302.

[15] B. Elena, G. de Paëpe, L. Emsley, *Chem. Phys. Lett.* **2004**, *398*, 532 – 538.

[16] S. J. Clark, M. D. Segall, C. J. Pickard, P. J. Hasnip, M. I. J. Probert, K. Refson, M. C. Payne, *Z. Kristallogr.* **2005**, *220*, 567 – 570.

[17] C. Pickard, F. Mauri, *Phys. Rev. B* **2001**, *63*, 245101.

Received: January 19, 2015
Published online: March 25, 2015

